JOURNAL OF GEOPHYSICAL RESEARCH, VOL. 115, B06311, doi:10.1029/2009JB006700, 2010

Kinematic and seismic analysis of giant tabular iceberg breakup at Cape Adare, Antarctica

Seelye Martin,[1] Robert Drucker,[1] Richard Aster,[2] Fred Davey,[3] Emile Okal,[4] Ted Scambos,[5] and Douglas MacAyeal[6]

Received 30 June 2009; revised 20 January 2010; accepted 29 January 2010; published 18 June 2010.

[1] Satellite imagery reveals that a series of large icebergs (B15B in April 2001, C19 in June 2003, and B15A in October 2005) broke up or fractured while exiting the Ross Sea in a narrowly defined area off Cape Adare, Antarctica. Examination of recent swath-mapped bathymetric observations revealed that the principle agent of these breakups is a previously unknown 9 km long ridge with minimum depths of 215 m that we call Davey Shoal. Satellite imagery shows that the icebergs are driven into the shoal by coastal currents that converge over the narrow continental shelf. One of the icebergs, the 120 km by 30 km B15A, was instrumented with a seismograph, GPS, and fluxgate compass. This instrumentation provided a unique opportunity to establish the details of the iceberg kinematics that were not revealed by satellite imagery alone and to correlate seismic events observed both on the iceberg and in the far field during breakup. B15A fractured from multiple strikes against Davey Shoal and the adjacent Possession Islands; these strikes were driven by the combination of tidal currents and the coastal mean flow. The periods of iceberg-sourced seismic radiation were correlated with the strikes. The iceberg- and land-based seismic signals showed that the iceberg fracture, its sliding across the shoals, and the ice-on-ice stick-slip contacts among the postbreakup iceberg fragments generated the strong chaotic and harmonic tremor episodes that were observed at distances as far as the South Pole, where these signals propagated as seismically coupled hydroacoustic T phases.

Citation: Martin, S., R. Drucker, R. Aster, F. Davey, E. Okal, T. Scambos, and D. MacAyeal (2010), Kinematic and seismic analysis of giant tabular iceberg breakup at Cape Adare, Antarctica, *J. Geophys. Res.*, *115*, B06311, doi:10.1029/2009JB006700.

1. Introduction

[2] The consequences of grounding contact between drifting icebergs and the seabed are of interest to a variety of glaciological, sedimentological, oceanographic, biological and paleoclimate research areas [*MacAyeal et al.*, 2006; *Kooyman et al.*, 2007; *Smale et al.*, 2008]. In the case where grounding leads to iceberg breakup, the resulting dispersal of fragments modifies the pattern and timing of iceberg melting and subsequent impact on ocean thermohaline structure. Grounding also has the capacity to locally erode marine sediment on the continental margins and to displace seafloor biota at depth ranges that are not influenced by other marine erosion processes. Finally, grounding and iceberg-iceberg collisions are a source of seismic and hydroacoustic energy that can be monitored at stations far from iceberg sources to determine processes, rates and patterns of iceberg fracture [*Talandier et al.*, 2002, 2006; *Ruiz*, 2003; *MacAyeal et al.*, 2008a, 2009]. A challenge associated with such studies is that large icebergs calve infrequently from the Antarctic ice shelves. Since the advent of satellite remote sensing and for the Ross Sea, the recent calving of large icebergs from the Ross Ice Shelf since 2000, and the calving of B9 in the late 1980s [*Keys et al.*, 1990] represent the best examples of such calving events [e.g., *Vinje*, 1980; *Orheim*, 1980; *Long et al.*, 2001, 2002]. Also, as part of the broader SOUTHBERG study of iceberg behavior [*Okal and MacAyeal*, 2006; *MacAyeal et al.*, 2008a, 2008b], icebergs, including B15A, were equipped with onboard GPS, compass and seismographic instrumentation. As B15A encountered the Cape Adare shoals, the combination of newly acquired seabed topography, remote sensing imagery, onshore seismograph stations and iceberg-mounted instrumentation presented the opportunity to observe in unprecedented detail, the interac-

[1]School of Oceanography, University of Washington, Seattle, Washington, USA.
[2]Department of Earth and Environmental Science and Geophysical Research Center, New Mexico Institute of Mining and Technology, Socorro, New Mexico, USA.
[3]GNS Science, Lower Hutt, New Zealand.
[4]Department of Geological Sciences, Northwestern University, Evanston, Illinois, USA.
[5]National Snow and Ice Data Center, CIRES, University of Colorado at Boulder, Boulder, Colorado, USA.
[6]Department of Geophysical Sciences, University of Chicago, Chicago, Illinois, USA.

0148-0227/10/2009JB006700

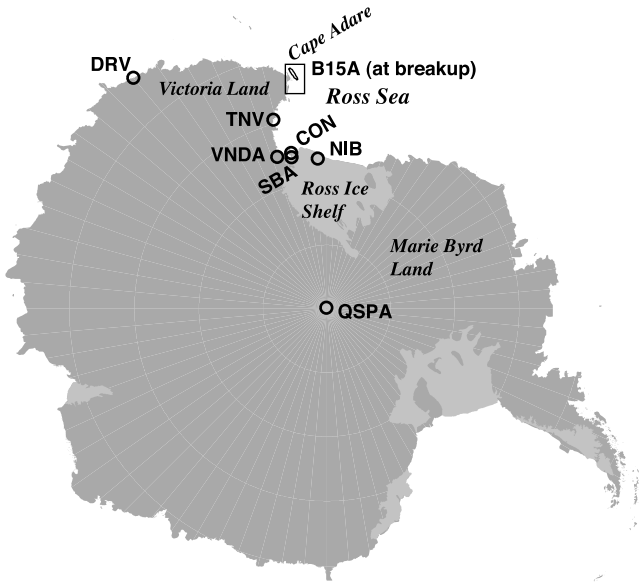

Figure 1. Map of Antarctica showing the geographic regions and seismic station locations referred to in this study. Box near Cape Adare shows the location of the bathymetric chart in Figure 2a and the size of iceberg B15A. The circles show the seismic stations discussed in the paper: DRV, Dumont d'Urville; TNV, Terra Nova Station; CON, Truncated Cones site on Mount Erebus; NIB, Nascent Iceberg (a station on the edge of the Ross Ice Shelf); SBA, Scott Base; VNDA, Lake Vanda; QSPA, South Pole.

tions of large icebergs with the seabed. It also allowed for the observation of the generation and propagation of seismic and hydroacoustic signals associated with the iceberg grounding and fracture.

[3] Recently, four large tabular icebergs (B9, B15B, C19, and B15A) broke up or fractured in the vicinity of Cape Adare while exiting the Ross Sea (Figure 1). For icebergs exiting the Ross Sea, there are at least two characteristic trajectories, both of which pass Cape Adare. The first is along the west side of the Ross Sea, in the current that carries the cold ice shelf water to the north. This occurred for C19 in 2003 and B15A in 2005. When these icebergs reach the continental shelf break, they are transported westward by a coastal current that flows approximately along the 500 m isobath past Cape Adare. The second is north and west in the central Ross Sea, where the icebergs encounter the same westward current at the shelf break, which also transports them past Cape Adare. This occurred for icebergs B9 in 1989 [*Keys et al.*, 1990, Figure 9] and B15B in 2001 [*Arrigo et al.*, 2002, Figure 1].

[4] Our first objective is to summarize and discuss the breakup and fracture of icebergs at Cape Adare. Examination of the breakup of B15A, as well as the breakup or fracture of B15B and C19 (detailed in the auxiliary material), reveal that these fracture events are associated with two geographic features: a shoal recently discovered from multibeam sonar data that is sufficiently strong (of hard rock origin; hereafter referred to as the "Davey Shoal") to severely damage icebergs that come into contact with it and the shoals around the Possession Islands, hereafter referred to as the "Possession Shoals."[1]

[5] These icebergs are exceptionally large. For example just prior to breakup, B15A measured 120 km in length and had a characteristic width of about 40 km. We are not as certain about the iceberg thicknesses. For icebergs that calve from the Ross Ice Shelf, *Dowdeswell and Bamber* [2007, Table 1 and Figure 3c] used radar altimeter data to measure iceberg freeboard and derive keel depths of 255 ± 50 m, where the depths have a peak in the range 250–300 m. For B15A, D. D. Blankenship (private communication, 2005) found from radar echo sounding a north side thickness of about 250 m and a south side thickness of 180 m. Using equations (1) and (2) of *Dowdeswell and Bamber* [2007] yields drafts of 210 and 120 m.

[6] In a previous discussion of the breakup of B15A, *MacAyeal et al.* [2006] noted that it was associated with the arrival of storm-generated sea swell from a particularly large storm in the Gulf of Alaska, which they hypothesized might have influenced the breakup. In the present paper, newly acquired bottom topographic data, combined with the detailed observations of the interaction of B15A with the shoals and the resultant seismic data, make it much more likely that the principal cause of the breakup was the iceberg collisions with Possession and Davey Shoals.

[7] The second objective is to report on the seismic signals produced during the breakup of B15A and the propagation of these signals to remote locations. Seismic data collected in situ on the iceberg, as well as at locations hundreds to thousands of kilometers away, help identify the mechanical nature of iceberg/seabed interactions. Iceberg tremor has been observed previously at land- and iceberg-based seismographs in Antarctica [*Ruiz*, 2003; *Müller et al.*, 2005; *Eckstaller et al.*, 2007, *MacAyeal et al.*, 2008a], on islands in the Southern Ocean [*Jansen and Müller*, 2008], and as far away as the equatorial Pacific [*Talandier et al.*, 2002, 2006]. In the present case, we find that the tremor is associated with iceberg-on-seabed and iceberg-on-iceberg collision processes associated with stick-slip behavior along a contact surface and with fracture of the iceberg. Our observations and analysis do not categorically rule out other sources of iceberg tremor that have been proposed to explain cases where tremor radiates from freely floating icebergs in deep water, as occurs with fluid flow vibrations in glacial conduits [*Talandier et al.*, 2006; *Jansen and Müller*, 2008]. Understanding the seismic signals associated with iceberg breakup and collision processes, offers the potential to monitor breakups with remote seismic measurements and to better understand iceberg collisions and fracture.

2. Seabed Bathymetry off Cape Adare

[8] Figure 2 shows charts of regional bathymetry from *Davey and Jacobs* [2007], showing Cape Adare, the Possession Islands and within the black box, the newly discovered Davey Shoal (Figures 2b and 3). Figure 2 shows the steep offshore drop in depth at the edge of the continental

[1] Auxiliary materials are available in the HTML. doi:10.1029/2009JB006700.

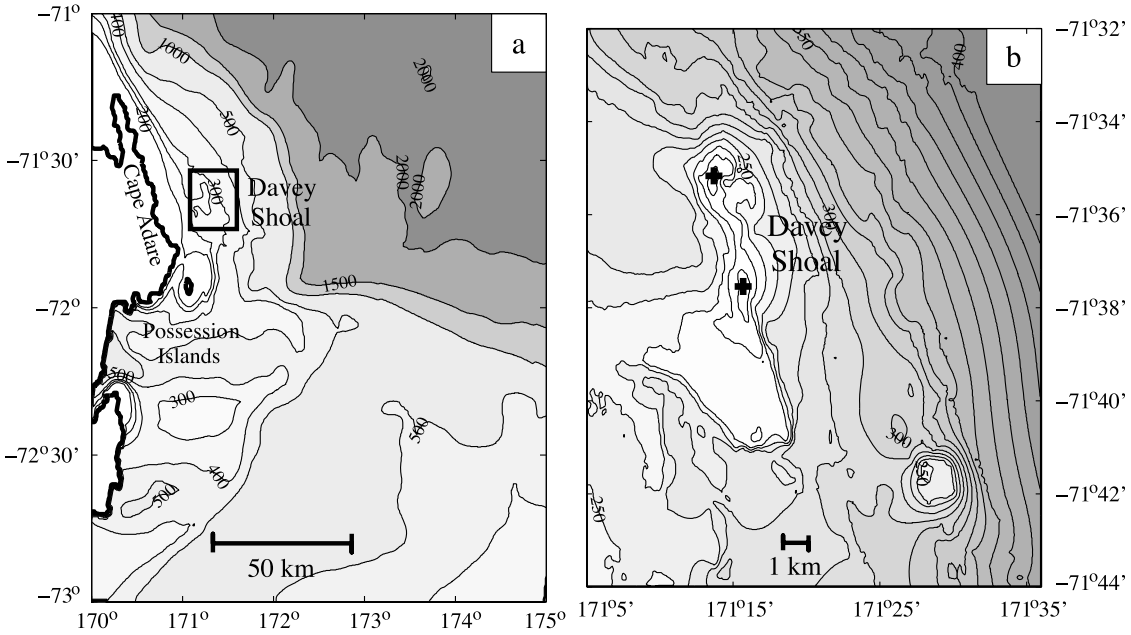

Figure 2. Bathymetric maps of the northwest Ross Sea showing Cape Adare, the Possession Islands, and the major bathymetric features, as derived from multibeam sonar bathymetry and single-channel bathymetric surveys. (a) Regional bathymetry, contours at 100 m intervals on the continental shelf (to 600 m depth). Black rectangle shows extent of Figure 2b. (b) Detailed topography of the shoal, contours at 10 m intervals. The small crosses on Davey Shoal mark the two topographic summits with depths of 216 m. Data courtesy of Land Information New Zealand and R/V *Nathaniel B. Palmer* multibeam surveys.

shelf and the convergence of the shelf toward the northern tip of the cape. Examination of the 250 m contour on Davey Shoal shows that the north-south ridge is roughly parallel to Cape Adare and is about 12 km long, or small compared to the 120 km length of B15A. A detailed examination of the topography shows that the shoal has two summits, to the north and in the middle, both with depths of 216 m. About 8 km southeast of the southern end of the shoal, there is

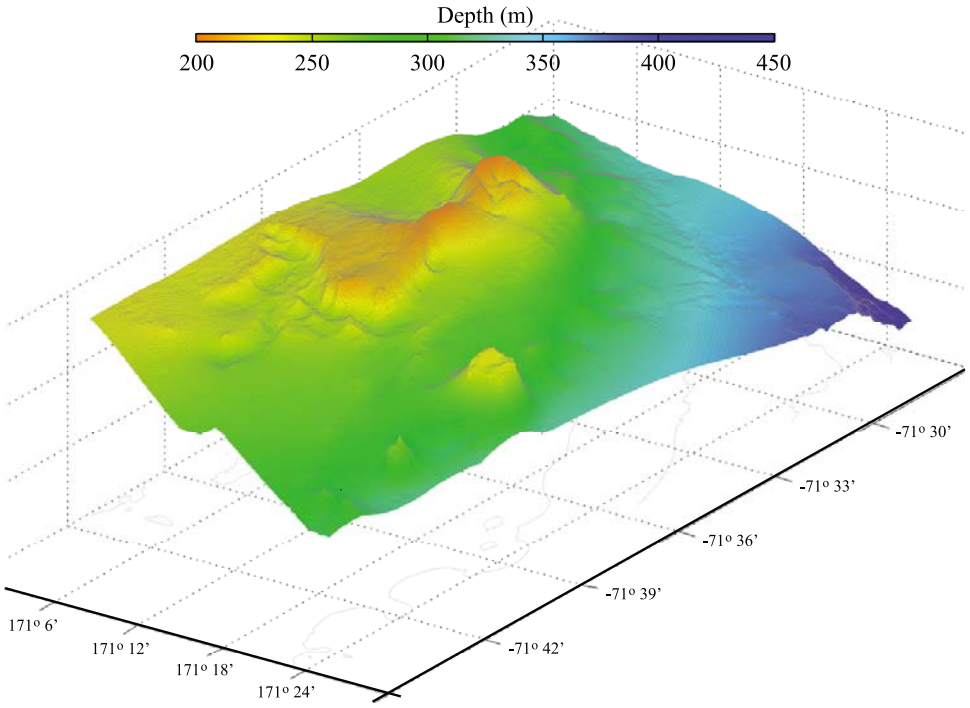

Figure 3. Three-dimensional perspective view of Davey Shoal and the seamount off Cape Adare in Figure 2 as viewed from the southeast.

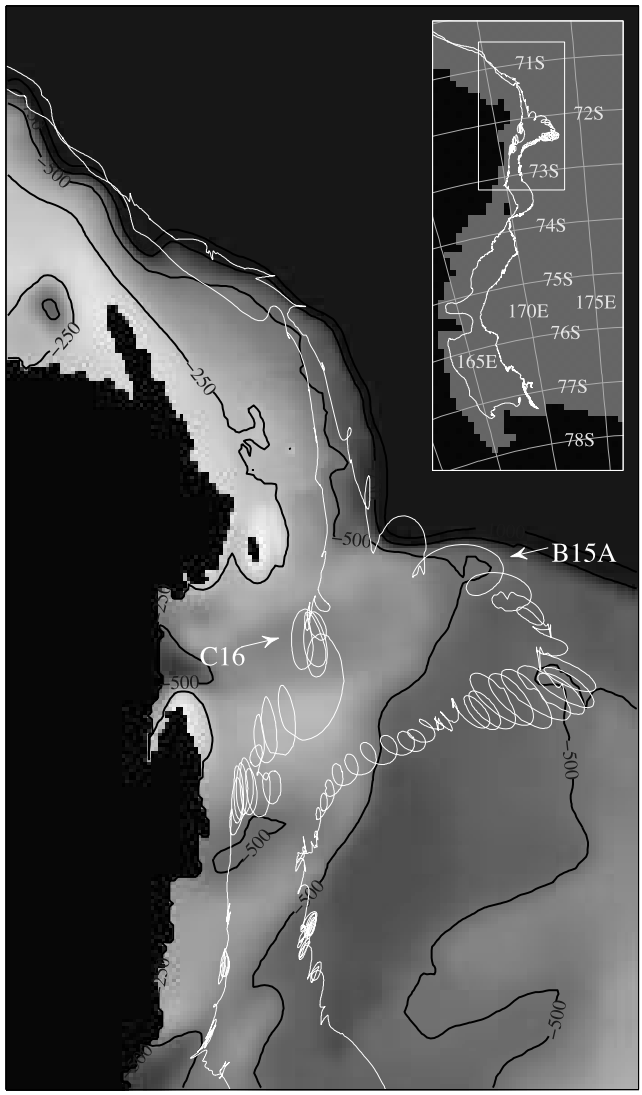

Figure 4. Convergence of the trajectories for the transit of icebergs B15A and C16 past Cape Adare. The inset shows an overall view of the iceberg tracks out of the Ross Sea. Trajectories represent paths of GPS stations deployed on the icebergs. See text for further description.

a flat-topped seamount with a minimum depth of 247 m and a summit diameter of about 1.5 km. The different minimum depths of these two features, and whether the icebergs clear them, allow us to place limits on the iceberg depths.

[9] Regional aeromagnetic data [*Damaske et al.*, 2007] do not show a magnetic anomaly associated with either the shoal or the seamount, indicating that unlike Cape Adare, they are not of volcanic origin, but are probably formed of indurated Paleozoic Robertson Bay Group metasediments [*Läufer et al.*, 2006], which are found onshore west of Cape Adare. These sediments may have been uplifted to form the ridge during the east-west rifting that formed the Adare Basin [*Cande et al.*, 2000] and the present continental shelf edge.

[10] Figure 4 shows the trajectories at 20 min intervals of GPS-equipped automatic weather stations (AWS) mounted on icebergs B15A and C16 as they transited Cape Adare. C16, which had a length of 40 km, a width of about 15 km and a maximum thickness of 75 m, did not fracture at Cape Adare, probably because it was too thin to ground on Davey Shoal [*MacAyeal et al.*, 2008a]. Within the Ross Sea, as B15A and C16 approached Cape Adare and the western exit of the Ross Sea, their daily motion was amplified into a series of large loops with the period of a diurnal tidal cycle. The loops are driven by the intensification of topographic vorticity component of the tide over the northern continental shelf of the Ross Sea [*Whitworth and Orsi*, 2006; *Padman et al.*, 2008; *MacAyeal et al.*, 2008a].

[11] Prior to reaching Cape Adare, B15A and C16 display dissimilar, independent drift trajectories. As they approach Cape Adare, the narrowing of the continental shelf and resultant constriction of the westward directed, bathymetric parallel shelf current forces the two icebergs to follow nearly the same trajectory, while the diurnal looping decreases noticeably. Specifically, the two trajectories are about 50 km apart during the approach to Cape Adare, but on reaching the Cape, they differ by less than 10 km (a distance possibly accounted for by the relative positioning of the GPS on the iceberg surfaces; thus, not refuting the possibility that the trajectories of the center of areas of each iceberg differ by even less). This trajectory convergence is likely a general phenomena because the narrowing of the continental shelf imposes potential vorticity constraints that, as *Padman et al.* [2008] show, traps the current between the shore and the shelf break. Given that the long-term mean drift trajectories and tidal oscillations around this mean are less variable in the vicinity of Cape Adare than within the Ross Sea suggests that the icebergs off Cape Adare will follow unidirectional drift trajectories and if deep enough, will encounter the shoals. This further suggests that over the long-term, icebergs exiting this region of the Ross Sea have completely denuded the shoal and seamount of surface sediments, rendering them rocky and hard, and a navigational hazard to icebergs.

3. Breakup of Icebergs Observed by Satellite

[12] The most remarkable and consistent iceberg/seabed interaction displayed by the satellite imagery involves the fracture of icebergs in the vicinity of Cape Adare. In temporal order, the affected bergs include B9, B15B, C19, and B15A. For B15A, B15B, and C19, we used data from the visible/infrared Moderate Resolution Optical Imaging Spectrophotometer (MODIS) instrument on AQUA and TERRA; for B9 in 1989, the first documented iceberg to breakup off Cape Adare, we rely on the work by *Keys et al.* [1990], who use advanced very high resolution radiometer (AVHRR) data to describe the breakup.

[13] The approximate time of the breakup or fracture of B15A, B15B, and C19 was determined from the University of Wisconsin Web site (http://ice.ssec.wisc.edu). We then searched the NASA Earth Observing System Data Gateway for the cloud-free MODIS images closest in time to the breakup or fracture. These images were converted to geographically registered images that were plotted over the bottom topography.

[14] Intercomparison of the satellite imagery associated with the three recent iceberg breakups showed remarkable consistency as to where they fractured (the auxiliary material

discusses B9, B15B, and C19; B15A is discussed below). In response to collisions with Davey Shoal, each iceberg fractured at approximately the same location. This consistency drew our attention to the possible existence of a previously unrecognized shoal in the area and to the possibility that iceberg interaction with the shoal caused the breakup of B15A.

[15] Prior to this study, one could argue that iceberg breakup was largely a stochastic process that neither favored certain locations nor certain iceberg properties. The overall significance of the remarkable consistency between the fracture events associated with B15A, B15B, C19, and B9, where B15B, C19, and B9 are discussed in the auxiliary material, is that for Cape Adare, icebergs tend to breakup in a deterministic manner in the vicinity of Davey Shoal.

4. Encounter of Iceberg B15A With the Shoals

[16] In support of our description of the breakup of B15A, we have data from 250 m resolution MODIS imagery and from an iceberg-mounted GPS, a Hall effect compass, and a seismograph, as well as complementary seismic records from Antarctic stations. The auxiliary material describes the instruments in detail. The iceberg-mounted instruments were deployed from McMurdo by helicopter and Twin Otter over the 2003 and 2004 field seasons. Data from the GPS and compass were telemetered via the ARGOS satellite data system. Data from the seismograph could not be transmitted via satellite, and so depended on a special data recovery mission in November 2005 conducted by a Twin Otter flight from McMurdo. The GPS and compass were left on the iceberg and continued to function until approximately July 2007, when their fragment of B15A melted.

[17] A difficulty in correlating seismic events with the drift and rotation of B15A, was that the Hall effect digital compass on B15A had a nonlinear response and needed to be calibrated a posteriori. The auxiliary material describes this calibration, which was performed by comparing compass readings with iceberg orientations derived from satellite imagery.

[18] As the trajectory in Figure 4 shows, B15A drifted out of the Ross Sea, then followed the coastal topography past Cape Adare. Within Ross Sea, it rotated 180° so that its thick side, which was the side furthest from the ocean while the iceberg was still part of the Ross Ice Shelf, encountered the shoals. During this encounter, Figure 5 shows four successive georegistered 250 m resolution MODIS images of the iceberg with the 250 m depth contour and land outline superimposed, at times noted on the images. The white dot marks the location of the instrument package, determined by plotting the GPS position on the georegistered images. Figures 5a and 5b show the iceberg before fracture. In the 18 h between the two images, the iceberg has pivoted around Davey Shoal and away from Possession Shoals where, as we show below, Figure 5a shows the maximum iceberg incursion of the iceberg onto these shoals. Figure 5c shows that 6 h after Figure 5b, the iceberg has fractured into four large pieces, with the fracture centered at the shoal. Four days later, Figure 5d shows that an additional large piece has fractured off, and that the constraints of the shoal and the largest piece of the iceberg prevent some of the fractured pieces from moving to the northwest. Figure 5 also shows that the iceberg drifted over the small seamount and fractured on Davey Shoal, suggesting that its depth was less than 250 m and greater than 215 m.

[19] In Figures 5c and 5d, the long linear shapes of the postbreakup pieces suggest that breakup was accommodated by mode 1 (tensional) propagating fractures, likely abetted by bottom crevasses that formed parallel to the Ross Ice Shelf front before the iceberg calved. Such features can be expected to result in an anisotropic bulk strength that influences the geometry of iceberg breakup [*Thomas and MacAyeal*, 1982; *Thomas et al.*, 1984; *Peters et al.*, 2007]. *MacAyeal et al.* [2008b, Figure 1] show a MODIS image from November 2004 of a similar long-axis fracture of B15A near Ross Island.

4.1. Correlation of the Seismic Signals With Iceberg Drift

[20] The interaction of B15A with the shoal took place in the 2 day period between 26 October 1000 UTC and 28 October 0600 UTC. We document this interaction in two ways: first, by examination of the iceberg motion and its interactions with the shoals; second, by examining the associated seismic activity recorded on the iceberg.

[21] For 26 October, 1000 UTC, to 28 October, 0200 UTC, Figures 6a–6f show the B15A motion in outline form at hourly intervals as determined from the GPS and the corrected compass heading. On Figures 6a–6f, land is black, the dark line shows the 250 m contour, the dots show the hourly GPS positions and the white lines are the hourly outlines of the iceberg. In Figures 6a–6f, the brightness of the white lines increases with time. For comparison, Figure 7 shows the vertical component spectrogram for the breakup period observed by the seismograph on B15A with the associated seismogram beneath it. The horizontal time axis extends from 26 October, 1200 UTC, to 28 October, 1200 UTC. The short vertical lines labeled 5a–5c mark the times of the images in Figure 5a–5c; the gray horizontal lines labeled 6b–6e correspond to the periods shown in Figures 6b–6e. The seismic episodes shown in Figure 7 are labeled A–F.

[22] For 26 October, 1000 to 1400 UTC, Figure 5a shows the approach of B15A to Davey Shoal, a period with no notable seismic activity on the iceberg. In Figure 5b (26 October, 1400–1800 UTC), the iceberg encounters Davey Shoal in a glancing blow. The spectrogram and seismogram of Figure 7 shows that the associated seismic activity, labeled episode A, begins at 26 October, 1415 UTC, suggesting that the iceberg is in contact with the shoal. Following this encounter, Figure 6c (26 October, 1800 UTC, to 27 October, 0400 UTC) shows that B15A ceased its westward motion and began a clockwise rotation around Davey Shoal, such that the south end of the iceberg rides over the 250 m contour surrounding the Possession Islands. The iceberg reaches its maximum incursion onto the shoal at 27 October, 0400 UTC, which is about the time of the image in Figure 5a. Episode B in Figure 7 occurred as the iceberg rode up on the shoal.

[23] Around the period of maximum excursion, episode C shows that strong seismic activity occurred on the iceberg that was, as we show below, also recorded at far-field seismic stations, implying that the iceberg underwent powerful interactions with the bottom. Figure 6d (27 October, 0400–2100 UTC), shows that the iceberg begins a counter-

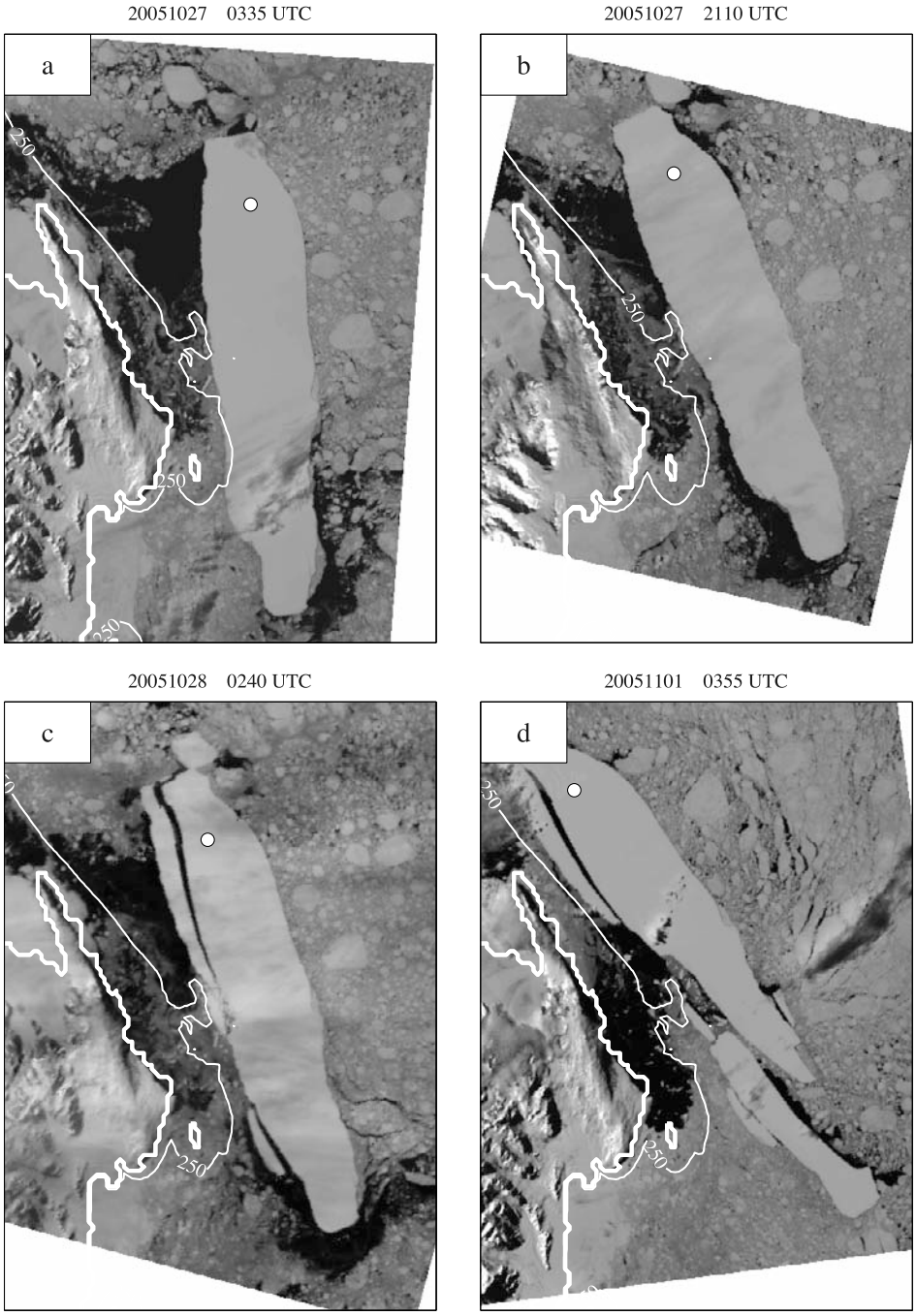

Figure 5. Four successive 250 m resolution MODIS images of B15A transiting Cape Adare, with associated times given at the top of each image. The thin white line shows the 250 m depth contour; the thick white line shows the coast; the white dots show the location of the instrument package. See text for further description.

clockwise rotation around Davey Shoal and moves off the Possession Shoals. As the iceberg moves off these shoals, episode C ceases and, with the exception of a short seismic burst in episode D, the iceberg transits to the northwest while remaining in contact with Davey Shoal without additional strong seismic tremor. This northwest transit continues until 27 October, 2100 UTC; Figure 5b shows the image of the iceberg at about this time.

[24] In Figure 6e (27 October, 2100 UTC, and 28 October, 0200 UTC), the iceberg again rotates clockwise around Davey Shoal, generating episode E in Figure 7. At 28 October 0140 UTC, episode E ends and F begins, where the nature of the associated seismic signals changes dramatically from a nonharmonic chaotic spectrum to a harmonic spectrum with a greatly reduced amplitude. In the auxiliary material, these differences can be heard in audio files of

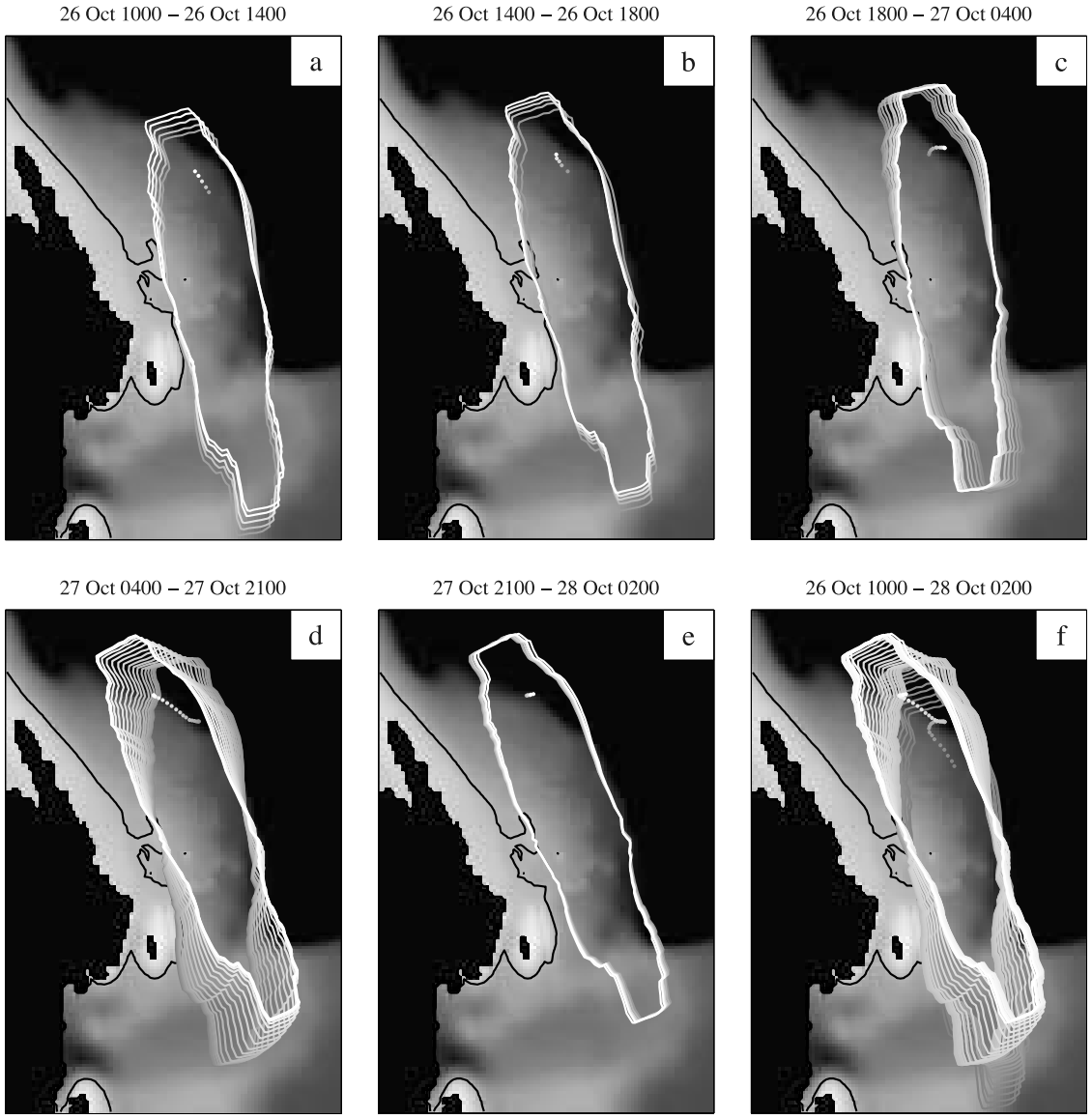

Figure 6. Sequential positions of iceberg B15A at 1 h intervals near Cape Adare. The white outlines show the iceberg positions. White dots show the location of the instrument package and, in each frame, the brightness of the outlines and dots increases with time. The black contour shows the 250 m contour and the topography is shaded so that deeper regions are darker. (a) 26 October, 1000–1400 UTC, the approach of the iceberg to Davey Shoal; (b) 26 October, 1400–1800 UTC, continued transit of the iceberg to the west, showing apparent shoal contact. (c) 26 October, 1800 UTC, to 27 October, 0400 UTC, iceberg pivots clockwise around shoal and has its closest approach to Possession Shoal at 0400 UTC. (d) 27 October, 0400 UTC, to 27 October, 2100 UTC, iceberg pivots counterclockwise around shoal, off Possession Shoal, and transits northwest. (e) 27 October, 2100 UTC, to 28 October, 0200 UTC, iceberg rotates clockwise around shoal, and fractures about 0130 UTC. (f) 26 October, 1000 UTC, to 28 October, 0200 UTC, summary image of iceberg displacement and rotation.

episodes C and E/F, where the seismic files are speeded up by a factor of 100. This suggests that as detailed below, the iceberg has fractured into several pieces, where stick-slip events between these pieces generate a harmonic signal. The MODIS images in Figures 5b and 5c confirm that between 27 October, 2100 UTC, and 28 October, 0240 UTC, the iceberg fractured along its long axis on the shoal. Finally, Figure 6f summarizes the hourly positions between 26 October, 1000 UTC, and 28 October, 0200 UTC, and shows that throughout the entire period, the iceberg remains in contact with Davey Shoal.

4.2. Details of the B15A Seismic Episodes

[25] Figure 8 shows detailed B15A spectrograms for the tremor episodes described in Figure 7. The episodes can be classified into two categories: chaotic and harmonic.

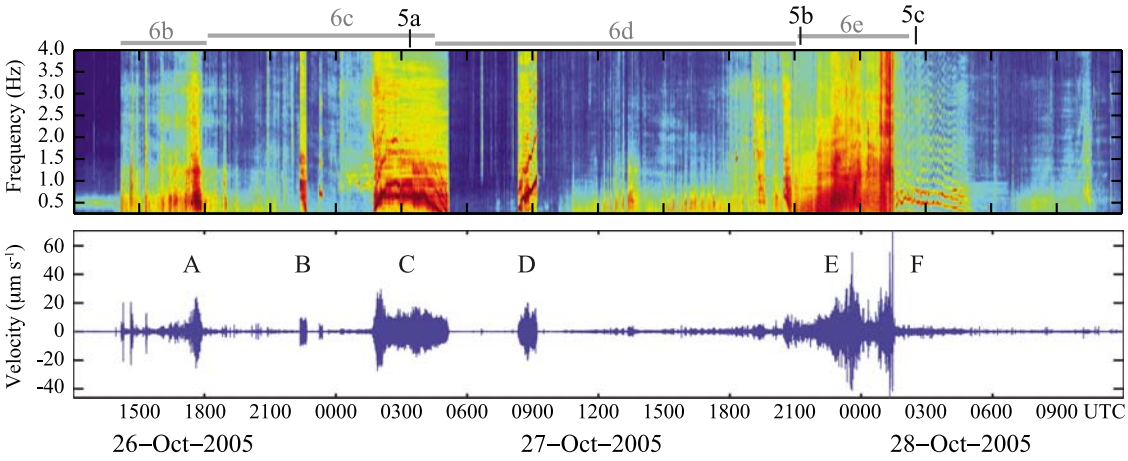

Figure 7. Forty-eight hour spectrogram observed by the B15A seismograph at the site shown on Figures 5 and 6, with the vertical component seismogram shown below. The horizontal time axis extends from 26 October, 1200 UTC, to 28 October, 1200 UTC. The spectrogram color scale depicts self-scaled logarithmic spectral amplitude calculated in 50% overlapping 512-sample (25.6 s) moving windows applied to decimated (20 samples/s) data with a spectrum estimated at 400 frequencies between 0.25 and 5 Hz. The times of the MODIS images in Figures 5a–5c are marked at the top; the gray horizontal lines show the duration of the iceberg trajectories in Figures 6b–6e. A–F on the seismogram identify the tremor episodes.

Chaotic tremor, most notable during episodes A and E, consists of highly variable, broadband signals in the seismic short-period range between approximately 1 to at least 25 Hz. We suspect that such episodes represent periods of multisource radiation arising from overlapping fractures, nonrepeatable short-duration episodes of basal slip and intraiceberg faulting events, and are likely characteristic of irreversible processes that weaken the iceberg. In the initiation of episode A, and during the iceberg fracture in episode E, aperiodic and high-energy, short-duration (10 s or less) broadband transients suggestive of fracture with frequency content up to and beyond 4 Hz, occur. These are particularly apparent in Audio S2 of episode E/F in the auxiliary material.

[26] Also as described in the auxiliary material, analysis of particle motion observed by the three-component seismograph on B15A revealed a polarization consistent with a source location at or near Davey Shoal. The polarization was strongly elliptical with a strike aligned with the presumed source-to-receiver direction. This is consistent with primarily P waves or T-P coupled seismic waves arriving at the seismograph site in which the particle motions are aligned with the source-receiver direction and strongly confined to the horizontal plane [*MacAyeal et al.*, 2008a]. At times throughout the various tremor episodes, a transverse polarization emerged, consistent with secondary tremor sources that became active after the multiple fragments of the postbreakup iceberg began to rub against each other. While the polarization is consistent with a tremor source located at Davey Shoal, the seismogram did not reveal distinct subevents for any of the tremor episodes, as was the case in the study of tremor on iceberg C16 reported by *MacAyeal et al.* [2008a]. The lack of subevent resolution for B15A is consistent with the relatively strong attenuation and scattering expected for the approximately 75 km, source-to-receiver distance on B15A relative to *MacAyeal et al.* [2008a], which incorporated four seismographs at distances from the source ranging from tens of meters to about 50 km.

[27] Harmonic tremor is identified in the spectrograms by the presence of harmonically spaced spectral lines (e.g., episodes B, C, D, F). *MacAyeal et al.* [2008a] demonstrate that this type of tremor arises (but not necessarily exclusively) from repetitive stick-slip subevents, where the fundamental frequency is the subevent repeat rate. In this process, harmonic "gliding," where the spectral lines change frequency with time, tends to track changes in the subevent repeat rate, and is correlated with the iceberg velocity and presumably with other frictional characteristics of the contact. From the B15A record, we suspect that harmonic tremor also arises from relatively nondestructive repetitive basal stick slip between icebergs and the seabed.

[28] Figure 9 shows the correlation between the iceberg motion and seismic events as an annotated time series of GPS positions. The small circles show the GPS positions at 20 min intervals, where the colored circles show the location of the major seismic events as marked by their episode letters, the black circles mark specific events, such as a change in the rotation direction, and the annotations (5a, 5b, 5c) show the times of the MODIS images. The compass was recorded at 18, 38 and 58 min after the hour; for Figure 9, we have rounded these to 20, 40, and 60 min. Figure 9 shows a trajectory characterized by long linear drifts that are separated by cusps and a right-angled turn. Episode A occurs during an extended drift to the northwest as the iceberg first interacts with Davey Shoal. The iceberg next rotates onto the Possession Shoals, where the cusp at 27 October, 0400 UTC, occurs when the iceberg is at its maximum incursion. The harmonic tremor episodes B and D are approximately symmetric relative to the cusp, and the powerful episode C occurs at the cusp during a period of practically zero motion (i.e., although episode C is 255 min long (27 October, 0145–0530 UTC), it occupies only four

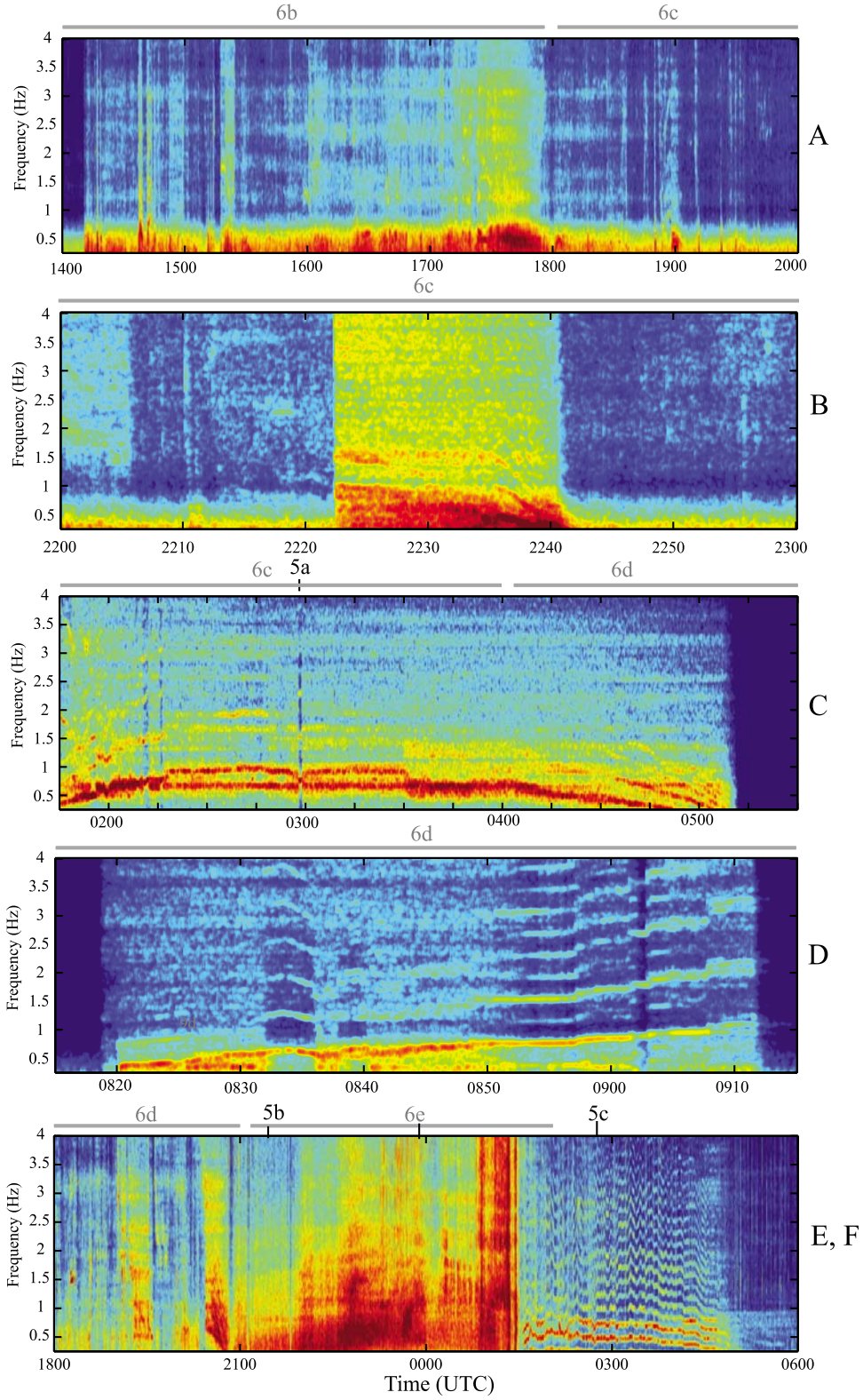

Figure 8. Expanded spectrograms on different time axes for tremor episodes identified and annotated in Figure 7, recorded by the seismograph on B15A showing detailed time-frequency evolution of collisions leading to B15A breakup. Episode A, primarily chaotic, low-frequency tremor with weak harmonic components. Episodes B and C, complex harmonic tremor with multiple voices. Episode D, gliding, primarily harmonic tremor. Episode E, chaotic, relatively high frequency tremor during iceberg breakup. Episode F, gliding harmonic tremor, postbreakup.

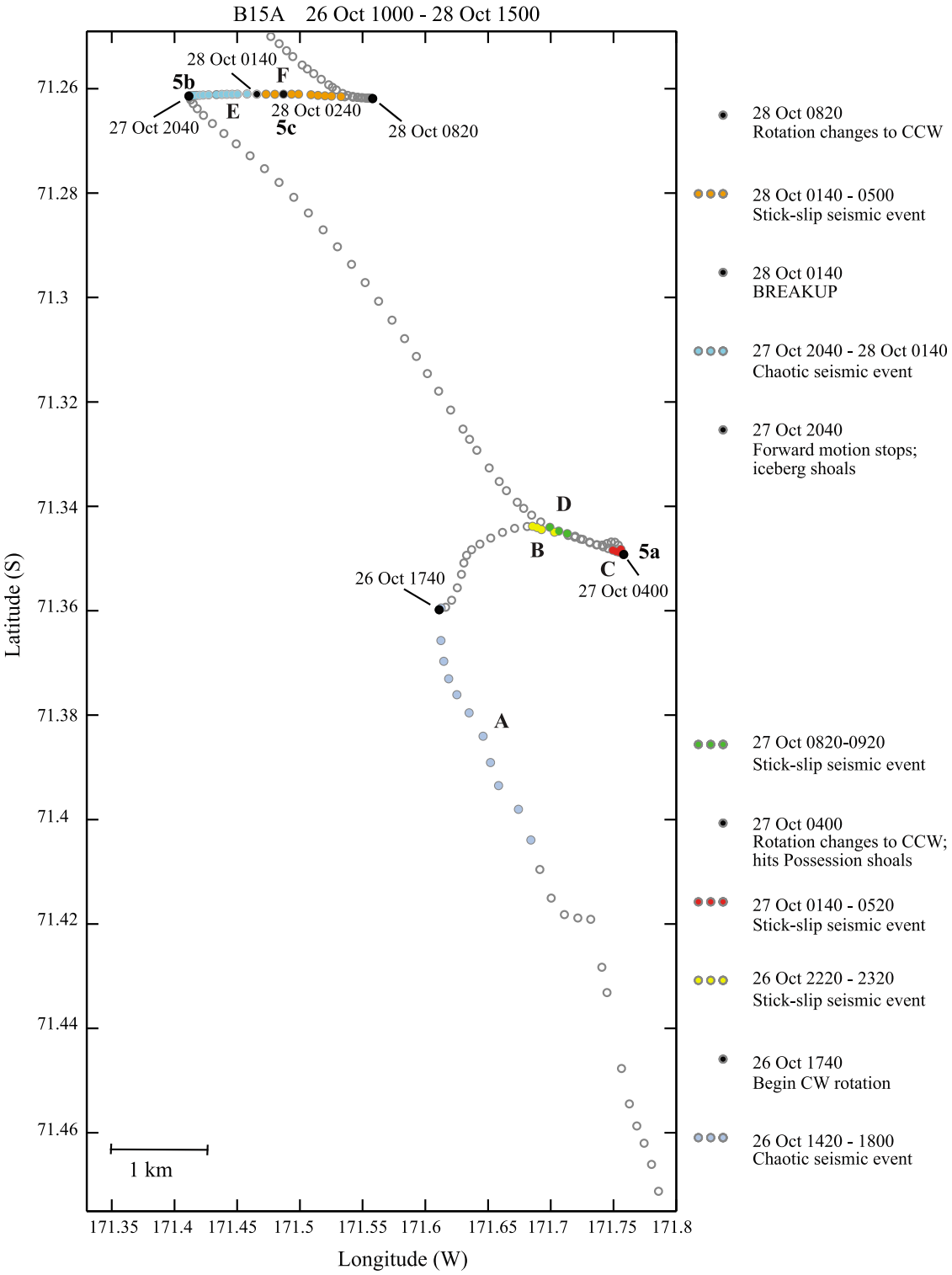

Figure 9. GPS position of the B15A instrument package at 20 min intervals. The colored dots show the location of the seismic events, described to the right, and the letters show the location of the MODIS images in Figure 5. The colors are chosen for contrast only. A–F are the times of the tremor episodes shown in Figures 7 and 8.

circles on Figure 9). Following another period of linear drift, the abrupt right turn at 27 October, 2040 UTC, occurs just before breakup at the beginning of chaotic episode E. The second cusp at 28 October, 0820 UTC, occurs after the iceberg has fractured and, as Figure 7 shows, at this time, there is only weak seismic activity.

[29] In Figure 8, examination of episode C shows a period of harmonic tremor with a fundamental frequency compo-

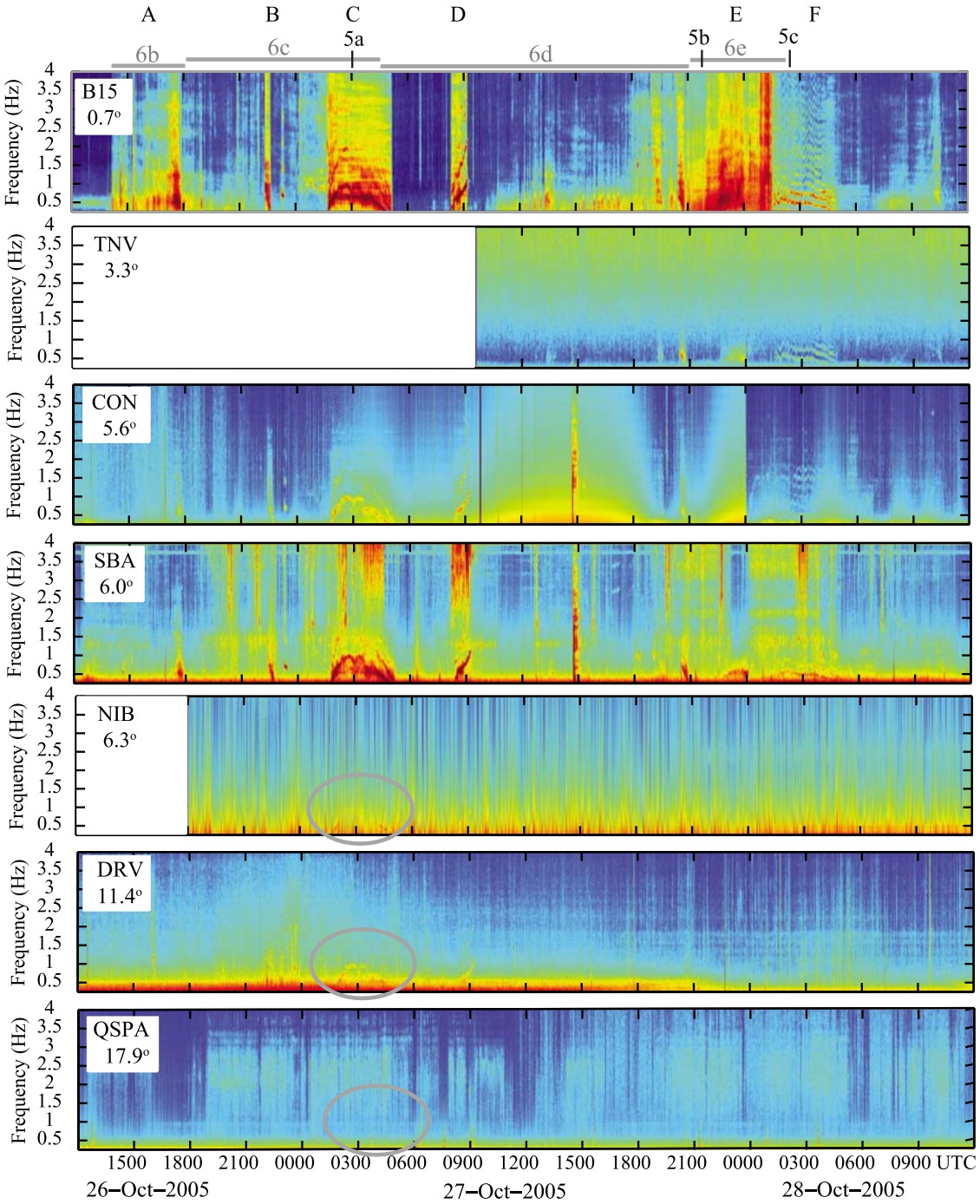

Figure 10. Forty-eight hour vertical component spectrograms of the B15A breakup from the B15A seismograph and the Antarctic stations shown in Figure 1. On the left, the station abbreviations and approximate distance from the source-to-station in degrees are listed, assuming that the separation between the sensor and the source region on B15A is 0.7°. The spectrograms show varying signal-to-noise ratios. The ellipses show the location of tremor episode C at the most distant stations where the signals are faint. At the most distant station, QSPA, the seismic signals are invisible in this depiction.

nent that increases from below 1 Hz to above 1.5 Hz at the midpoint of the episode, and then glides back down to below 1 Hz by the end. The initial part of this tremor episode has multiple harmonic voices, which can be identified by multiple tracks of nonharmonically related spectral lines. This suggests that because the iceberg is grounded against both shoals, a number of stick-slip sites are active, producing the observed multiple voices. There is an abrupt spectrogram power minimum near 0300 UTC that is close to the time when the iceberg reaches its maximum extent onto the shoal. This is similar to the aseismic tremor "eye" features reported by *MacAyeal et al.* [2008a] for cessation

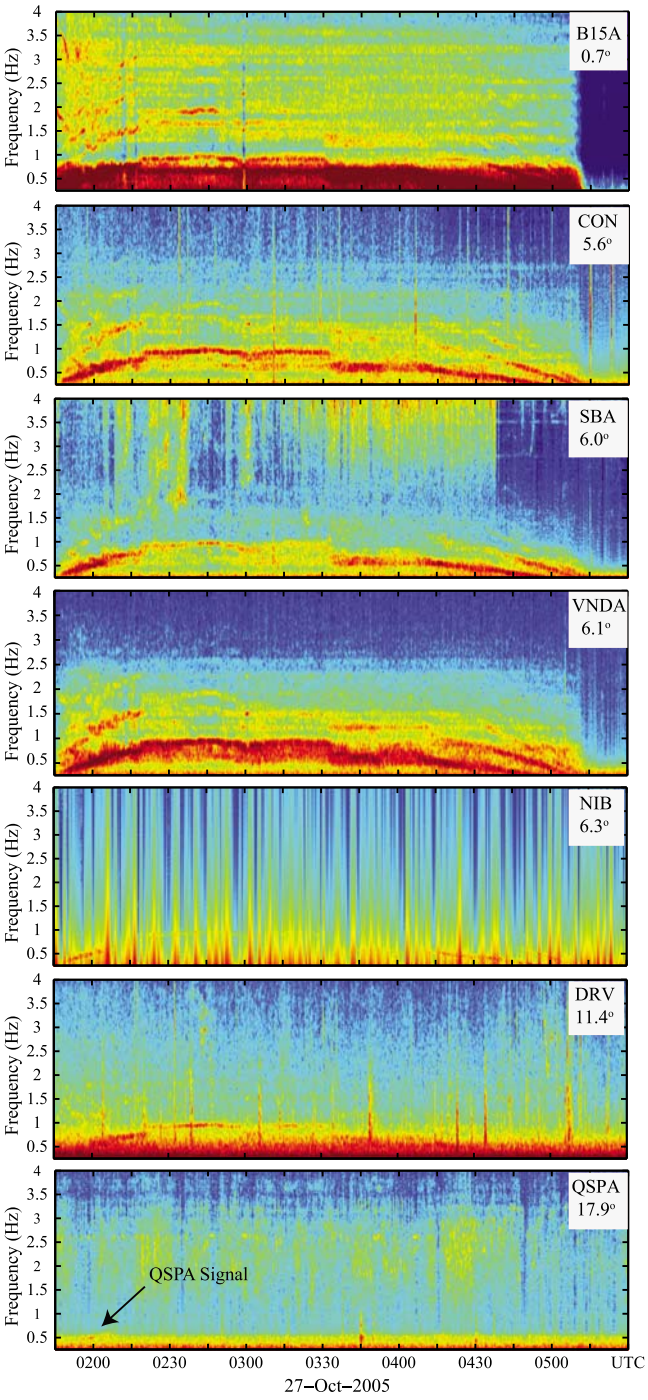

Figure 11. Propagation of seismic signals from tremor episode C (Figures 7 and 8) to Antarctic seismometer stations (Figure 1) on B15A (−71.34, 171.72, mean values during episode). The stations are Mount Erebus (CON; −77.54, 167.09), Scott Base (SBA; −77.85, 166.76), Lake Vanda, Dry Valleys (VNDA; −77.52, 161.85), Nascent Iceberg (−78.13, 178.50), Dumont d'Urville (−66.67, 140.01), and South Pole (−89.93, 145.00), with estimated source-receiver distances noted in degrees. The relatively faint and low-frequency signal at QSPA is marked with an arrow.

periods of iceberg-iceberg stick slip between B15A and C16 in 2003. However, in this case the spectrogram eye does not coincide with a gradual decrease in harmonic frequencies, as was the case with the relatively geometrically and dynamically simple case of glancing collision iceberg tremor [*MacAyeal et al.*, 2008a].

[30] The next major seismic event in Figures 7 and 8 is chaotic tremor episode E. As Figure 9 shows, this occurs as the iceberg stops drifting northwest, and again begins to pivot clockwise around Davey Shoal (Figures 5b and 5c). This chaotic tremor is of higher frequency (above 10 Hz) than that observed previously and includes numerous transients, particularly toward its end. It begins about 27 October, 2040 UTC, at the abrupt right turn in the GPS trajectory and continues until 28 October, 0130 UTC, when it switches abruptly to episode F, a relatively low-amplitude, nearly pure harmonic signal. The transients and broadband signal from episode E are associated with the final stages of breakup, consistent with the abrupt propagation of fractures that extend throughout the body of the iceberg. In contrast, we suspect that the harmonic tremor in episode F arises from the post-fracture repetitive lateral stick slip between two of the large B15A fragments via the mechanism of *MacAyeal et al.* [2008a]. The presence of a single set of harmonics during this episode indicates a single predominant source. The polarization of particle motions (see the auxiliary material) for this episode is also consistent with a source that is in a different location than the previous shoal contact episodes.

4.3. Regional and Teleseismic Signals Associated With the Breakup of B15A

[31] Although not directly relevant to the issue of characterizing the iceberg tremor source processes, we next investigate the teleseismic propagation of the tremor signals to remote stations in Antarctica (and elsewhere, but without signal receipt) as a means of characterizing their propagation modes. The breakup of B15A was detected at a number of remote seismic stations. Figure 10 shows vertical component seismic spectrograms for the entire B15A breakup period as recorded on B15A and at the locations shown on Figure 1, specifically Terra Nova Station (TNV), Truncated Cones (Mount Erebus; CON; [*Aster et al.*, 2004]), Scott Base (SBA), Nascent Iceberg (NIB; a floating iceberg station near the edge of the Ross Ice Shelf [*Okal and MacAyeal*, 2006]), and Dumont d'Urville (DRV) and South Pole (QSPA), where the seismometer is located in a 300 m deep borehole 8 km from South Pole station [*Park et al.*, 2005]. Although for QSPA, which is located at 17.9° from the iceberg, the signal from the most far-ranging episode C is invisible in this depiction, as we show below, this signal is readily recoverable with filtering. Spurred by prior identification of the hydroacoustic T phase propagation of iceberg tremor as far as the South Pacific [*Talandier and Okal*, 1998; *Talandier et al.*, 2002, 2006], we additionally searched without success for associated signals at other stations in the southern hemisphere, including CASY (Casey Station, Antarctica), RAR (Raratonga), RAO (Raoul Island, NZ), RPN (Rapa Nui, Easter Island), PPT (Tahiti), MCQ (MacQuarie Island), and PAF (Kerguelen Island).

[32] For episode C and the various seismic stations, Figure 11 shows seismic spectrograms of the most energetic

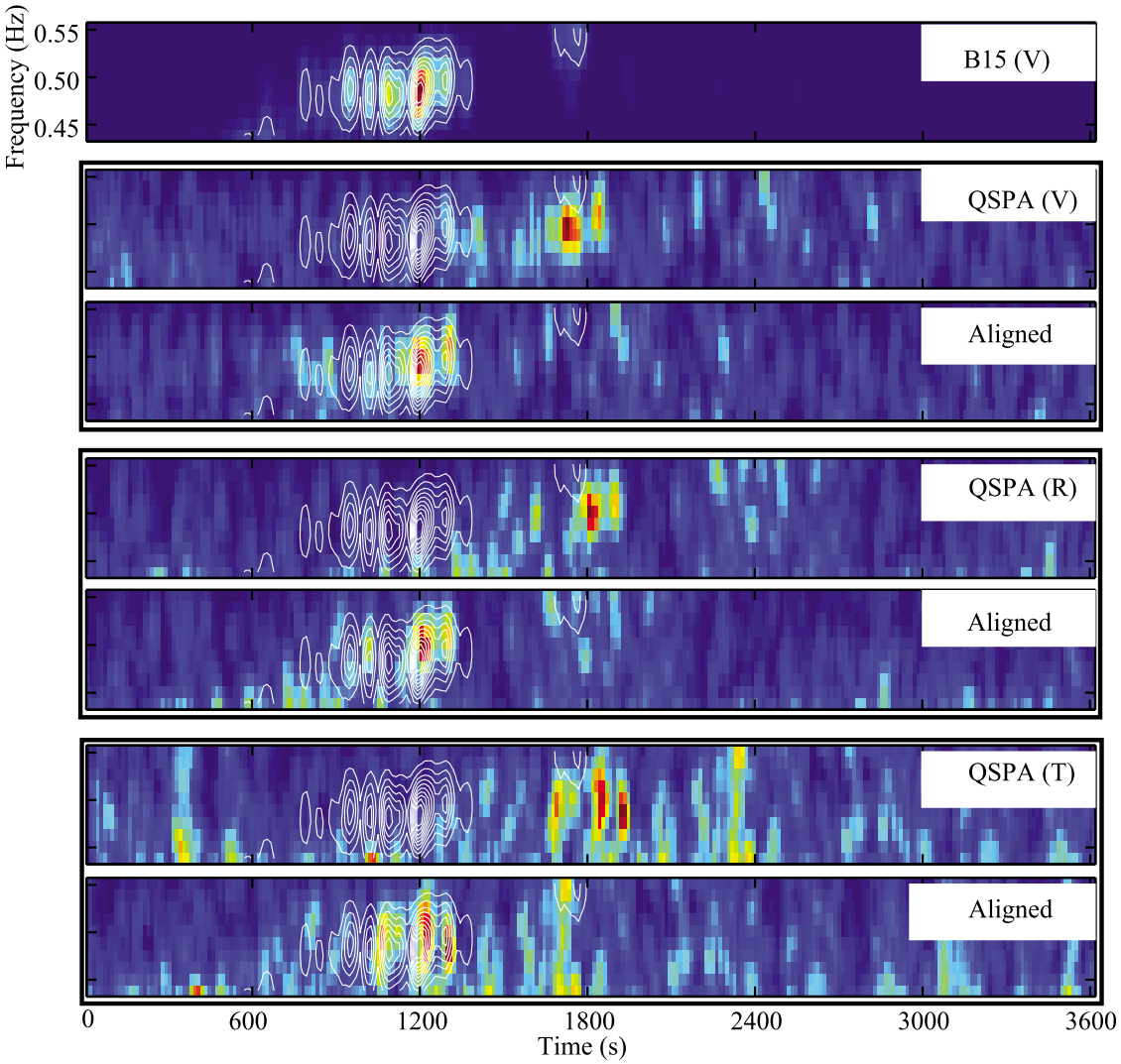

Figure 12. Spectrogram correlation (spectral energy; not spectral amplitude logarithm as in earlier spectrograms) of diagnostic low-frequency signals near the onset of tremor episode C recorded at B15A and on vertical (V), radial (R), and tangential (T) polarized components of seismic station QSPA, with each component shown overlain and aligned by the best lag, defined as the maximum of the sum of the 10 constituent frequency bin correlations. All white contours are from the QSPA spectrogram to assist in demonstrating alignments.

low-frequency (sub-1 Hz fundamental) events. Because of its large-amplitude, low-frequency, and low-attenuation properties, as well as the presence of an identifiable spectral structure and energetic subevents, episode C is particularly valuable for studying the regional to teleseismic (greater than approximately 1,000 km) propagation of the iceberg harmonic tremor. The stations in Figure 11 are similar to those in Figure 10, with the exception of TNV, which was inactive during this episode, and with the addition of VNDA (Lake Vanda, Dry Valleys), even though it was intermittently operational. Unlike Figure 10, the episode is now visible at all stations.

[33] For seismic waves generated by shallow sources, regional seismic wave propagation at ranges up to several hundred km is complex. The complexities arise because of strong scattering due to the heterogeneity of the crust and at frequencies above a few Hz, to the heterogeneity of the topography as well, and to the interaction of the waves with the crustal waveguide bounded by the free surface and the Moho crust-mantle boundary [e.g., *Kennett*, 1989]. The identification of constituent phases in iceberg tremor is further complicated by the quasi-continuous nature of the source.

[34] To investigate the regional propagation modes of iceberg tremor, we used spectrogram correlation, which takes advantage of the spectral "fingerprinting" [e.g., *Hedlin et al.*, 2002; *Talandier et al.*, 2002] arising from tremor source transients and the spectral gliding of harmonic components. For episode C and the 1 h period beginning on October 27 at 0145 UTC, which includes its high-amplitude, low-frequency initiation, we partially deconvolved the short-period response of the B15A vertical seismogram and used its spectrogram as a fingerprint to correlate with signals from distant seismic stations. Where station configurations

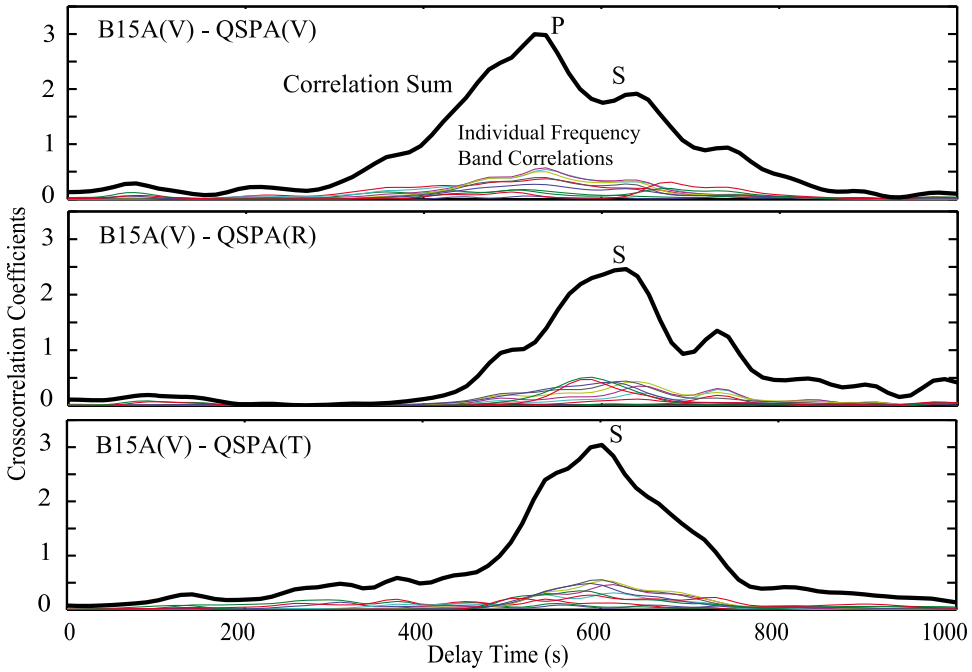

Figure 13. For episode C, the spectrogram correlation functions between B15A and the vertical (V), source radial (R), and source tangential (T) components of QSPA (Figure 12), showing 10 individual spectrogram frequency band correlations separated in center frequency by 0.0125 Hz and their corresponding sums. Spectrogram frequency bands used for correlations of tremor episode C arrivals at various stations (Figure 1) were established based on graphical examination of the signal-to-noise of the distant station QSPA: 0.43 – 0.55 Hz (10 bands); SBA, CON: 0.24 – 0.55 Hz (16 bands); VNDA: 0.24 – 1.0 Hz (61 bands); DRV: 0.46 – 0.64 Hz (15 bands); NIB: 0.36 – 0.68 Hz (16 bands). The final estimate of the lag is determined by the mean best lag and its standard deviation is estimated from the scatter of the best lags of the individual frequency bands.

and data quality permitted, we rotated the horizontal components into radial and tangential components to attempt to separate P-S coupled waves in the vertical plane (P-S_V) from tangentially polarized S waves (S_H) that should be less affected by P-S coupling. Figures 12 and 13 show examples of the spectrogram correlation results for QSPA, the most distant station at which we detected this signal. In Figure 13, the consistent delay of the radial and tangential correlations and the prominent initial peak for the vertical correlation is suggestive of the detection of P and S waves. We identify probable P and S phases from the correlations of the B15A signal with the vertical and two (rotated) horizontal components, showing a "P" travel time of 529 ± 11 s and an "S" travel time of 615 ± 23 s. We performed similar analyses for the other stations in Figure 11.

[35] To estimate transit times between the iceberg source and the various stations in Antarctica where the signal was received, we assumed a source location that corresponds with the iceberg's initial fracture location, i.e., about 75 km south of the seismic station on B15A, and that the timing of the source signal is equivalent to that of the signal received at the seismic station on B15A corrected for the iceberg's P wave velocity (about 2.925 km s^{-1} [*MacAyeal et al.*, 2008a]). Figure 14 compares the resulting transit times with the appropriate seismic velocities [*Kennett and Engdahl*, 1991] and with a hydroacoustic T phase sound speed of 1.5 km s^{-1}. As the travel times show, the tremor phases are significantly delayed by 100–300 s relative to the pure P and S body phases predicted by the global average IASPEI91 velocity model of *Kennett and Engdahl* [1991]. At regional distances of approximately 1° to 7°, the signals are also delayed relative to the crustal waveguide L_g phase that dominates continental path seismograms from shallow sources within this range. We conclude that all remotely observed signals incorporate an initial slower propagating T phase leg in their paths, and that these T phases are converted to seismic phases at variable and perhaps multiple points along the Antarctic coast before being observed at the remote stations. The transmission of converted T phase events for significant distances into the interior of continents has been observed elsewhere and modeled (e.g., in Europe by *Cansi and Bethoux* [1985]).

[36] The influence of the T phase leg is demonstrated most clearly at the sole continental interior station, QSPA, where the inferred P and S phase arrival times (Figures 12, 13, and 14) are significantly delayed relative to the P and S direct travel time curves, and show a reduced S-P time difference for the full 17.9° distance relative to that predicted by direct P and S propagation. The observed S-P time difference at QSPA of approximately 86 s is consistent with a source-receiver distance of approximately 8° (Figure 14), which compares favorably with the range to that part of the Ross Sea coast nearest to the South Pole, at the western edge of the Ross Ice Shelf (Figure 1). However, for the simplest T to (P, S) conversion at this range, the absolute arrival times of the QSPA phases are about 300 s early, indicating that

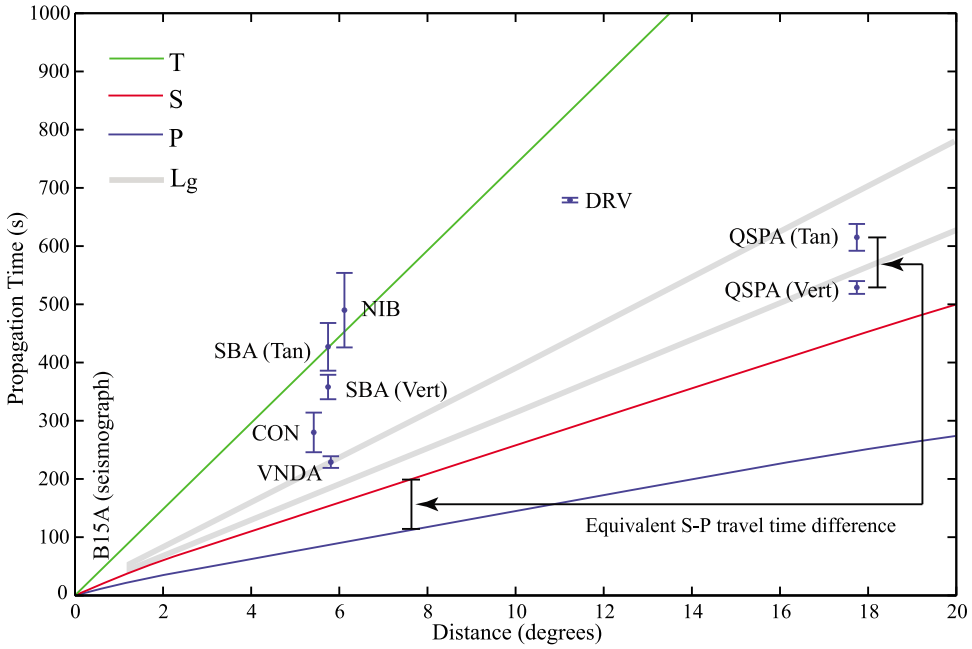

Figure 14. Propagation times for the low-frequency transient near the onset of tremor episode C at six Antarctic seismograph stations (locations in Figure 1) compared to IASPEI91 S and P travel times (red and blue lines), T phase hydroacoustic propagation (green line) and a representative range for the crustal phase L_g (gray lines). In all cases, the observed propagation times are delayed relative to S and P travel times, indicating a significant hydroacoustic leg along the propagation path. The arrival times at the most distant, inland station, QSPA, provide the most convincing evidence for the existence of the T phase leg. For this case, the arrow connects the observed S-P travel time difference with the theoretical value and shows that the theoretical value is less than half the observed. This suggests that the signal at QSPA converted from a hydroacoustic to a seismic phase in the southern reaches of the Ross Sea. See Figure 13 caption for a description of the derivation of the error bars.

additional crustal propagation and phase interconversion complexity and/or non-great circle propagation is required to explain the travel time data. Possible explanations are that despite their polarization signatures, the two phases are not in fact P and S, that the phases represent distinct T to seismic coupling regions that are geographically distinct, and/or that the T to seismic coupling is occurring at oceanic island sites or via other nongeodesic propagation paths.

[37] Although the great circle path for DRV (Figure 1) suggests the possibility of near-source T to body wave conversions, the arrival time of the energy unambiguously indicates a predominantly T phase propagation from B15A to DRV. This suggests high attenuation and/or poor T to seismic interconversion efficiency for a great circle path transiting Victoria Land, but is consistent with a T phase scattered off the Balleny Islands and converted at the continental shelf edge. Delays for Ross Island station SBA and the floating Ross Ice Shelf station NIB, which have the most unambiguous purely oceanic geometric paths, are both consistent with pure T phase propagation, although SBA also displays distinct vertical and tangential component arrivals that, as with QSPA, are inconsistent with simple T to body wave coupling scenarios at Ross Island and are instead suggestive of multiple conversion points. Stations CON on Mount Erebus, and VNDA, which is located tens of km from the coast and has the most nearly nonoceanic path to B15A, show faster propagation suggestive of an early T to seismic conversion.

[38] The interconversion efficiency of T phases to seismic waves is significantly controlled by the seafloor bathymetry, with steeper slopes favoring efficient conversion of T phases to solid Earth seismic phases [*Okal and Talandier*, 1997; *Talandier and Okal*, 1998]. This implies that the hydroacoustic waves radiated by an iceberg will not necessarily be converted to seismic phases at the closest coastline or island, but will instead be converted where the coastal geometry is favorable. Given the role of the T phase propagation, it remains an open question as to why this and other B15A breakup phases were not observed at more distant seismic stations, such as French Polynesia, where such phases had previously been detected from iceberg collisions. We suspect that the lack of these phases reflects the particular geographic location of the B15A source and the local SOFAR channel conditions.

5. Conclusions

[39] Using multibeam sonar, satellite remote sensing, iceberg geodesy, and oceanographic and seismic observations, the paper presents a detailed study of the breakup of a giant tabular iceberg B15A at Cape Adare. These observations, combined with the discovery of Davey Shoal, allow us to present a timeline of the interaction of B15A with Davey and Possession Shoals, along with its resultant seismic activity. A unique feature of this study is that the repeated groundings of B15A onto the shoals and its sub-

sequent breakup into fragments are correlated with the strength and nature of the seismic signals recorded on the iceberg and the Antarctic continent. These tremors are associated with stick-slip motions of icebergs rubbing on other icebergs, on hard rock of the seabed, and as transient seismic sources associated with iceberg fracture. The paper also confirms that basal ice-on-seabed stick-slip motion is a newly confirmed cause of iceberg harmonic tremor. Other source contribution mechanisms for iceberg-generated tremor (e.g., as described by *Jansen and Müller* [2008]) are not ruled out by our study; however, we conclude that these mechanisms did not occur during the breakup of B15A.

[40] Because the location of Davey Shoal in the "exit" of the Ross Sea on the narrow continental shelf off Cape Adare partially blocks the movement of icebergs along the shelf, this shoal and the adjacent Possession Shoals, are sites of concentrated iceberg/seabed interactions. These factors promote aggressive, iceberg-breaking denudation of the seabed, which appear to be in evidence at Davey Shoal, and provide a self-consistent explanation of its morphological features. Iceberg trajectories are funneled toward Davey Shoal by the dominant rectilinear currents and tides, so that icebergs exiting the Ross Sea consistently pass these shoals, where depending on thickness, some of them should fracture. Of the five icebergs described in the paper (including the auxiliary material), B9, B15B, C19, C16, and B15A, B9 broke up in the vicinity of Cape Adare, B15B and B15A fractured on the shoal, and C19 lost a small fragment in contact with the shoal. C16 did not fracture, probably because its shallow draft meant that it cleared the shoal. These observations support the hypothesis that the shoal, and the hard impacts that occur when icebergs attempt to negotiate it, are responsible for the fracture and breakup of large deep-draft icebergs exiting the Ross Sea.

[41] The seismometer data from B15A during its encounter with Davey and Possession Shoals allows for a unique view of breakup processes and dynamics that should help understand the complex seismic events radiating from floating ice in the Antarctic and Arctic. The most conspicuous element of the seismic recordings is the hours long tremor events exhibiting both harmonic and chaotic components, at times with embedded transients, associated with contact between B15A and the seabed. The evidence supporting this interpretation are (a) the timing of the tremor relative to the GPS and satellite-derived iceberg movements at the shoals, and (b) the tremors being sufficiently energetic to be observed at coastal and inland stations of Antarctica. Travel time correlations of the high-energy tremor components generated during breakup show delay times that indicate an initial transmission of hydroacoustic energy with subsequent coupling to seismic energy at and near the coast, where this coupling is sensitive to the geographic path and to the complicated coastal geography and bathymetry.

[42] The complexity of the tremor episodes indicates the occurrence of both transient ice fracturing and relatively nondestructive repetitive ice-seabed and ice-ice stick slip. The strong correlation between the iceberg motions relative to the shoals and breakup, and the iceberg tremor signals confirm that teleseismic tremor signals observed in the Pacific by *Talandier et al.* [2002, 2006], and in the present paper at the South Pole, are associated with icebergs undergoing processes that affect their dynamics and integrity. This suggests that in the future, systematic monitoring at remote stations of tremor from iceberg calving and interaction sites in the northern and southern hemispheres may serve as a way to quantify iceberg calving [*MacAyeal et al.*, 2009], movement and breakup, and motivate more sustained and geographically complete seismic and hydroacoustic monitoring of polar regions.

[43] **Acknowledgments.** S.M. and R.D. gratefully acknowledge the support of NASA under contract NNG04GM69G; D.R.M. gratefully acknowledges the support of NSF grant ARC-0907834.We thank David Long for help with QUIKScat iceberg trajectory data and Young-Jin Kim for originally alerting us to the possibility that B15A's breakup was associated with contact with seabed features and for assisting in the analysis of the compass data recovered from B15A. Instruments were provided by the Program for Array Seismic Studies of the Continental Lithosphere (PASSCAL) facility of the Incorporated Research Institutions for Seismology (IRIS) through the PASSCAL Instrument Center at New Mexico Tech. The Global Seismographic Network (GSN) is a cooperative scientific facility operated jointly by the Incorporated Research Institutions for Seismology, the USGS, and the National Science Foundation. All seismic data in this paper are available from the IRIS Data Management Center. IRIS facilities are supported by cooperative agreement NSF EAR-000430 and the Department of Energy National Nuclear Security Administration. Financial and logistical support was generously provided by the National Science Foundation (NSF) under grants OPP-0229546, OPP-0229492, OPP-0230028, OPP-0229305, and ANT-0538414. Land Information New Zealand kindly provided the critical multibeam bathymetric data. Referee and editor comments were greatly helpful toward substantially improving the manuscript and analysis.

References

Arrigo, K. R., G. L. van Dijken, D. G. Ainley, M. A. Fahnestock, and T. Markus (2002), Ecological impact of a large Antarctic iceberg, *Geophys. Res. Lett.*, *29*(7), 1104, doi:10.1029/2001GL014160.

Aster, R., et al. (2004), Real-time data received from Mount Erebus Volcano, Antarctica, *Eos Trans. AGU*, *85*(10), 97, doi:10.1029/2004EO100001.

Cande, S. C., J. M. Stock, R. D. Mueller, and T. Ishihara (2000), Cenozoic motion between East and West Antarctica, *Nature*, *404*, 145–150, doi:10.1038/35004501.

Cansi, Y., and N. Bethoux (1985), T waves with long inland paths: Synthetic seismograms, *J. Geophys. Res.*, *90*, 5459–5465, doi:10.1029/JB090iB07p05459.

Damaske, D., A. L. Läufer, F. Goldmann, H.-D. Möller, and F. Lisker (2007), Magnetic anomalies northeast of Cape Adare, northern Victoria Land (Antarctica), and their relation to onshore structures, in *Antarctica: A Keystone in a Changing World—Online Proceedings for the 10th International Symposium on Antarctic Earth Sciences, Santa Barbara, California, U.S.A.—August 26 to September 1, 2007*, edited by A. Cooper, C. Raymond, and the 10th ISAES Editorial Team, *U.S. Geol. Surv. Open File Rep.*, *2007-1047*, SRP 016, doi:10.3133/of2007-1047.srp016.

Davey, F. J., and S. S. Jacobs (2007), Influence of submarine morphology on bottom water flow across the western Ross Sea continental margin, in *Antarctica: A Keystone in a Changing World-Online Proceedings for the 10th International Symposium on Antarctic Earth Sciences, Santa Barbara, California, U.S.A.-August 26 to September 1, 2007*, edited by A. Cooper, C. Raymond, and the 10th ISAES Editorial Team, *U.S. Geol. Surv. Open File Rep.*, *2007-1047*, SRP 067, doi:10.3133/of2007-1047.srp067.

Dowdeswell, J. A., and J. L. Bamber (2007), Keel depths of modern Antarctic icebergs and implications for sea-floor scouring in the geological record, *Mar. Geol.*, *243*, 120–131, doi:10.1016/j.margeo.2007.04.008.

Eckstaller, A., C. Müller, L. Ceranna, and G. Hartmann (2007), The Geophysics Observatory at Neumayer stations (GvN and NM-II) Antarctica, *Polarforschung*, *76*(1–2), 3–24.

Hedlin, M., B. Stump, D. Pearson, and X. Yang (2002), Identification of mining blasts at mid- to far-regional distances using low frequency seismic signals, *Pure Appl. Geophys.*, *159*, 831–863, doi:10.1007/s00024-002-8661-7.

Jansen, D., and C. Müller (2008), Iceberg generated tremor in the vicinity of South Georgia Island, *Geophys. Res. Abstr.*, *10*, Abstract EGU2008-A-10824.

Kennett, B. L. N. (1989), On the nature of regional seismic phases-1. Phase representations for Pn, Pg, Sn, Lg, *Geophys. J. Int.*, *98*, 447–456, doi:10.1111/j.1365-246X.1989.tb02281.x.

Kennett, B. L. N., and E. R. Engdahl (1991), Travel times for global earthquake location and phase identification, *Geophys. J. Int.*, *105*, 429–465, doi:10.1111/j.1365-246X.1991.tb06724.x.

Keys, H. J. R., S. S. Jacobs, and D. Barnett (1990), The calving and drift of iceberg B-9 in the Ross Sea, Antarctica, *Antarct. Sci.*, *2*, 246–257, doi:10.1017/S0954102090000335.

Kooyman, G., D. Ainley, G. Ballard, and P. Ponganis (2007), Effects of giant icebergs on two emperor penguin colonies in the Ross Sea, Antarctica, *Antarct. Sci.*, *19*, 31–38, doi:10.1017/S0954102007000065.

Läufer, A. L., G. Kleinschmidt, F. Henjes-Kunst, F. Rossetti, and C. Faccenna (2006), Geological map of the Cape Adare Quadrangle, Victoria Land, Antarctica, 1:250,000, in *German-Italian Geological Antarctic Map Programme (GIGAMAP)*, edited by P. C. Pertusati and N. W. Roland, Bundesanst. für Geowis. und Rohstoffe, Hannover, Germany.

Long, D. G., M. R. Drinkwater, B. Holt, S. Saatchi, and C. Bertoia (2001), Global ice and land climate studies using scatterometer image data, *Eos Trans. AGU*, *82*(43), 503, doi:10.1029/01EO00303.

Long, D. G., J. Ballantyne, and C. Bertoia (2002), Is the number of Antarctic icebergs really increasing?, *Eos Trans. AGU*, *83*(42), 469, doi:10.1029/2002EO000330.

MacAyeal, D. R., et al. (2006), Transoceanic wave propagation links iceberg-calving margins of Antarctica with atmospheric storminess in tropics and northern hemisphere, *Geophys. Res. Lett.*, *33*, L17502, doi:10.1029/2006GL027235.

MacAyeal, D., E. A. Okal, R. Aster, and J. Bassis (2008a), Seismic and hydroacoustic tremor generated by colliding icebergs, *J. Geophys. Res.*, *113*, F03011, doi:10.1029/2008JF001005.

MacAyeal, D., E. A. Okal, J. Thom, K. Brunt, Y.-J. Kim, and A. Bliss (2008b), Tabular iceberg collisions within the coastal regime, *J. Glaciol.*, *54*(185), 371–386, doi:10.3189/002214308784886180.

MacAyeal, D., E. A. Okal, R. Aster, and J. N. Bassis (2009), Seismic observations of glaciogenic ocean waves (micro-tsunamis) on icebergs and ice shelves, *J. Glaciol.*, *55*(190), 193–206, doi:10.3189/002214309788608679.

Müller, C., V. Schlindwein, A. Eckstaller, and H. Miller (2005), Singing icebergs, *Science*, *310*(5752), 1299, doi:10.1126/science.1117145.

Okal, E. A., and D. MacAyeal (2006), Seismic recording on drifting icebergs: Catching seismic waves, tsunamis and storms from Sumatra and elsewhere, *Seismol. Res. Lett.*, *77*(6), 659–671, doi:10.1785/gssrl.77.6.659.

Okal, E. A., and J. Talandier (1997), T waves from the great 1994 Bolivian deep earthquake in relation to channeling of S wave energy up the slab, *J. Geophys. Res.*, *102*(B12), 27,421–27,437, doi:10.1029/97JB02718.

Orheim, O. (1980), Physical characteristics and life expectancy of tabular icebergs, *Ann. Glaciol.*, *1*, 10–15.

Padman, L., S. L. Howard, A. H. Orsi, and R. D. Muench (2008), Tides of the northwestern Ross Sea and their impact on dense outflows of Antarctic Bottom Water, *Deep Sea Res.*, *Part II*, doi:10.1016/j.dsr2.2008.10.026.

Park, J., et al. (2005), Performance review of the global seismographic network for the Sumatra-Andaman megathrust earthquake, *Seismol. Res. Lett.*, *76*, 331–343, doi:10.1785/gssrl.76.3.331.

Peters, M. E., D. D. Blankenship, D. E. Smith, J. W. Holt, and S. D. Kempf (2007), The distribution and classification of bottom crevasses from radar sounding of a large tabular iceberg, *IEEE Trans. Geosci. Remote Sens.*, *4*, 142–146, doi:10.1109/LGRS.2006.887057.

Ruiz, M. (2003), Analysis of tremor activity at Mt. Erebus Volcano, Antarctica, M.S. thesis, N. M. Inst. of Min. and Technol., Socorro.

Smale, D., K. Brown, D. Barnes, K. Fraser, and A. Clarke (2008), Ice scour disturbance in Antarctic waters, *Science*, *321*(5887), 371, doi:10.1126/science.1158647.

Talandier, J., and E. Okal (1998), On the mechanism of conversion of seismic waves to and from T waves in the vicinity of island shores, *Bull. Seismol. Soc. Am.*, *88*, 621–632.

Talandier, J., O. Hyvernaud, E. Okal, and P. Piserchia (2002), Long-range detection of hydroacoustic signals from large icebergs in the Ross Sea, Antarctica, *Earth Planet. Sci. Lett.*, *203*, 519–534, doi:10.1016/S0012-821X(02)00867-1.

Talandier, J., O. Hyvernaud, D. Reymond, and E. Okal (2006), Hydroacoustic signals generated by parked and drifting icebergs in the southern Indian and Pacific oceans, *Geophys. J. Int.*, *165*, 817–834, doi:10.1111/j.1365-246X.2006.02911.x.

Thomas, R., and D. MacAyeal (1982), Derived characteristics of the Ross Ice Shelf, Antarctica, *J. Glaciol.*, *28*, 397–412.

Thomas, R. H. R., D. MacAyeal, D. Eilers, and D. Gaylord (1984), Glaciological studies on the Ross Ice Shelf, Antarctica, 1973–1978, in *The Ross Ice Shelf: Glaciology and Geophysics*, *Antarct. Res. Ser.*, vol. 42, edited by C. R. Bentley and D. E. Hayes, pp. 21–53, AGU, Washington, D. C.

Vinje, T. (1980), Some satellite-tracked iceberg drifts in the Antarctic, *Ann. Glaciol.*, *1*, 83–87.

Whitworth, T., III, and A. H. Orsi (2006), Antarctic Bottom Water production and export by tides in the Ross Sea, *Geophys. Res. Lett.*, *33*, L12609, doi:10.1029/2006GL026357.

R. Aster, Department of Earth and Environmental Science, New Mexico Institute of Mining and Technology, 801 Leroy Pl., Socorro, NM 87801, USA.

F. Davey, GNS Science, PO Box 30368, Lower Hutt 5040, New Zealand.

R. Drucker and S. Martin, School of Oceanography, University of Washington, Box 357940, Seattle, WA 98195-7940, USA. (seelye@u.washington.edu)

D. MacAyeal, Department of Geophysical Sciences, University of Chicago, 5734 S. Ellis Av., Chicago, IL 60637, USA.

E. Okal, Department of Geological Sciences, Northwestern University, 1850 Campus Dr., Locy Hall, Evanston, IL 60208-2150, USA.

T. Scambos, National Snow and Ice Data Center, CIRES, University of Colorado at Boulder, 1540 30th St., Boulder, CO 80309-0449, USA.